J Mater Sci (2010) 45:5291–5301
DOI 10.1007/s10853-010-4574-5

Preparation and characterization of amino-functionalized nano-Fe_3O_4 magnetic polymer adsorbents for removal of chromium(VI) ions

Yong-Gang Zhao · Hao-Yu Shen · Sheng-Dong Pan · Mei-Qin Hu · Qing-Hua Xia

Received: 10 January 2010 / Accepted: 28 April 2010 / Published online: 14 May 2010

Abstract Four kinds of NH_2-functionalized nano magnetic polymer adsorbents (NH_2-NMPs) coupled with different diamino groups, i.e., ethylenediamine (EDA), diethylenetriamine (DETA), triethylentetramine (TETA), and tetraethylenepentamine (TEPA), named as EDA-NMPs, DETA-NMPs, TETA-NMPs, and TEPA-NMPs, respectively, have been prepared and characterized by transmission electron microscopy (TEM), X-ray diffractometer (XRD), vibrating sample magnetometer (VSM), elementary analyzer (EA), Brunauer, Emmett, Teller surface area analyzer (BET), and Fourier transform infrared spectroscopy (FTIR). The sorptive characteristics of the NH_2-NMPs intended for removal of chromium(VI) was investigated. Batch adsorption studies were carried out to optimize adsorption conditions. The evaluation of the adsorption kinetics, isotherm, and thermodynamics was deeply investigated. The results showed the adsorptive properties of the NH_2-NMPs were highly pH dependent. Adsorption of Cr(VI) reached equilibrium within 30 min. The data of adsorption kinetics obeyed pseudo-second-order rate mechanism well. The adsorption data for Cr(VI) onto NH_2-NMPs were well fitted to the Langmuir isotherm. The maximum adsorption capacities (q_m) of the NH_2-NMPs to Cr(VI) were 136.98, 149.25, 204.08, 370.37 mg g^{-1}, for EDA-NMPs, DETA-NMPs, TETA-NMPs, and TEPA-NMPs, respectively. Thermodynamic parameters like ΔH^{θ}, ΔS^{θ}, and ΔG^{θ} for the adsorption of Cr(VI) onto the NH_2-NMPs have been estimated, which suggested that the adsorption processes of Cr(VI) onto the NH_2-NMPs were endothermic and entropy favored in nature. The adsorption mechanism studies showed that the adsorption of Cr(VI) onto the NH_2-NMPs could be related with electrostatic attraction, ion exchange, and coordination interactions.

Y.-G. Zhao · H.-Y. Shen (✉) · S.-D. Pan · M.-Q. Hu
Ningbo Institute of Technology, Zhejiang University, Ningbo 315100, China
e-mail: hyshen@nit.zju.edu.cn

Y.-G. Zhao · S.-D. Pan
College of Science, Zhejiang University, Hangzhou 310027, China

Q.-H. Xia
Ministry-of-Education Key Laboratory for the Synthesis and Application of Organic Functional Molecules, School of Chemistry and Chemical Engineering, Hubei University, Wuhan 430062, China

Introduction

With the rapid development of global industrialization, more and more chromium, which has been placed on the top of the priority list of toxic pollutants by the U. S. EPA, has been applied in a wide range of industries, such as electroplating and metal finishing processes, tanning of leather, pigment and chemical industry, etc [1–3]. It is known that chromium has two main oxidation states, i.e., Cr(III) and Cr(VI), in aqueous systems. It has been reported that Cr(VI) is about 500 times more toxic than Cr(III) [3]. Several Cr(VI) compounds are toxic and act as carcinogens, mutagens, and teratogens in biological systems [4]. According to the reports of U. S. EPA, 97379 lb of chromium is released from surface water discharges and 29 million pounds is released due to dissolution from rain [5]. It is reported that the common concentrations of Cr(VI) found in wastewater are around 50–100 mg L^{-1}[6], which are over 1,000 times higher than the maximum allowed concentration (0.05 mg L^{-1}) in drinking water [7]. Therefore, more and more attention has been paid to develop an effective approach for the treatment of Cr(VI)-contained wastewater.

Some conventional methods [3], such as reduction, reverse osmosis, electrodialysis, ion exchange, and adsorption, have been used for this purpose. However, among these methods, few could achieve the discharge standards alone, and some of them even generated a large amount of secondary waste.

Relatively, adsorption is a conventional but efficient technique. Many kinds of adsorbents for wastewater treatment have been developed, such as activated carbon [8], activated alumina [9], coated silica gel [10], hydroxyapatite (HA)-based materials [11], peat moss [12], and raw rice bran [13]. However, how to separate the adsorbents quickly from the solution and shorten the separation time [14] are still the difficulties to be overcome. The features of magnetic adsorbents that can be subsided rapidly under a magnetic field provide an effective approach via magnetic separation [15]. Recently, Hu et al. reported a kind of magnetite (γ-Fe_2O_3) which was used for the removal of Cr(VI) ions from wastewater. Although this adsorbent could be separated rapidly from post-treatment wastewater system, its maximum adsorption capacity was only 17.0 mg g^{-1} [16]. In order to achieve high maximum adsorption capacity, various functional groups, including carboxylate, hydroxyl, sulfate, phosphate, amide, and amino groups, have been used to modify the conventional adsorbents [17, 18]. The surface functionalization of magnetic nanoparticles can be tailored if a chemical modification of polymeric shells is elaborately designed. Thus, selective adsorption on different metal ions can be realized [14, 19]. Amino-functionalized materials would be expected to be effective ones for removing heavy metals, since the removal of anionic metal species could not only be achieved via electrostatic interaction [20] or ion exchange [7] but also be realized via coordination interaction between metal ions and amino groups [21, 22]. However, reports on the preparation and application of NH_2-NMPs for the removal of Cr(VI) ion from wastewater were limited. Moreover, after modification with amino groups, the maximum adsorption capacity of the absorbents to the target heavy metal ions was not always improved as expected. For instance, the maximum adsorption capacity, for Cr(VI) ions, of the ethylenediamine-functionalized polymer, i.e., poly(GMA-*co*-MMA)-EDA, reported by Bayramoglu et al. [21], amino-functionalized magnetic nano-adsorbent, reported by Huang et al. [19], and the non-functional NMPs, reported by Hu et al. [16], was found to be 0.441 mmol g^{-1} (22.93 mg g^{-1}) [21], 11.24 mg g^{-1}[19], and 17.0 mg g^{-1}[16], respectively. Thus, to obtain novel NMPs with high adsorption capacity for heavy metal ions is still facing great challenges.

In this study, a series of novel NH_2-functionalized nano-sized magnetic polymer adsorbents (NH_2-NMPs) have been synthesized via the suspension polymerization followed by ring-opening reactions with different diamines, i.e., EDA, DETA, TETA, and TEPA, as illustrated in Fig. 1, named as EDA-NMPs, DETA-NMPs, TETA-NMPs and TEPA-NMPs, respectively. They were characterized by transmission electron microscopy (TEM), X-ray diffractometer (XRD), elementary analyzer (EA), Teller surface area analyzer (BET), Fourier transform infrared spectroscopy (FTIR), and vibrating sample magnetometer (VSM). The effectiveness of the NH_2-NMPs for the removal Cr(VI) from wastewater was verified from laboratory batch tests. Some important variables, e.g., the effects of pH value, the initial concentration of Cr(VI) solutions, were intensively investigated. The adsorption kinetics, thermodynamics, and adsorption isotherm were studied. Presumed mechanism of Cr(VI) adsorption onto NH_2-NMPs was also discussed. Some promising results were reported.

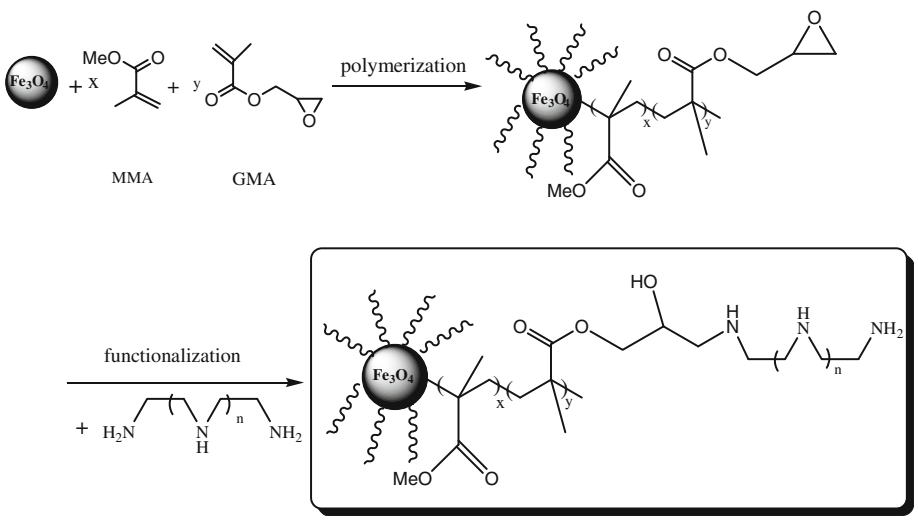

(n = 0, EDA-NMPs; n = 1, DETA-NMPs; n =2, TETA-NMPs; n = 3, TEPA-NMPs)

Fig. 1 A scheme for the binding and amino-functionalization procedure of NH_2-NMPs nanoparticles

Experimental section

Synthesis

All the necessary chemicals were of analytical grade and were purchased from the Sinopharm Chemical Reagent Co., Ltd. All the dilutions were prepared by ultrapure water.

Fe_3O_4 magnetic nanoparticles were prepared according to a reported procedure [23, 24] after minor modification. 1.0 g of Fe_3O_4 nanoparticles was dispersed in 200 mL ethanol under ultrasonication, then 5 mL of oleic acid was added dropwise under stirring at 80 °C for 1 h. The oleic acid-coated Fe_3O_4 nanoparticles (OA-M) were isolated in the magnetic field and washed with water and ethanol to remove redundant oleic acid.

The NH_2-NMPs were prepared by the following steps based on the suspension polymerization and ring-opening reactions. The preparation procedure of TEPA-NMPs was taken as an example for discussion.

2.0 g of polyglycol was dissolved into 200 mL hot water, followed by adding 4 mL (0.04 mol) methyl methacrylate (MMA) and 8 mL (0.05 mol) glycidylmethacrylate (GMA). Then 1.0 g of OA-M was dispersed to the above system under ultrasonication. Finally, 1.0 g of benzoyl peroxide (BPO) dissolved in 20 mL ethanol was added dropwise under vigorous stirring. The mixture was continuously reacted at 80 °C for 3 h, yielding M-*co*-(GMA-MMA) polymer. The resulting M-*co*-(GMA-MMA) was isolated under magnetic field and washed with water and ethanol to make it free from redundant GMA and MMA.

1.25 g of the M-*co*-(GMA-MMA) was dispersed into 50 mL methanol in a 100-mL flask. 15 mL of TEPA (0.08 mol) was added dropwise under stirring. The flask was then fitted with a water condenser and heated at 80 °C for 8 h. The final NH_2-NMPs were isolated under magnetic field and washed with water and methanol to pH value at ~7.0 to remove redundant diamines. The NH_2-NMPs were dried in a vacuum oven at 60 °C and stored in a sealed bottle for further use.

Characterization

The morphology and dimensions of the synthesized NH_2-NMPs were examined by a TEM (Hitachi H-7650) at 80 kV. Each sample was prepared by placing a very dilute particle suspension onto 400 mesh carbon grids coated with copper film. The structures of NH_2-NMPs were determined by an XRD (Bruker D8 Advance) at ambient temperature. The instrument was equipped with a copper anode generating Cu Kα radiation ($\lambda = 1.5406$ Å). Magnetic behavior was analyzed by a VSM (Lake Shore 7410). The surface area of the particles was measured by a BET (ASAP-2020) surface area analyzer. FTIR spectra were recorded on a Thermo Nicolet (NEXUS-470) FTIR spectrometer. Nitrogen percentage of NH_2-NMPs was analyzed with an elementary analyzer (EA) (ThermoFisher Flash-1112). Fe_3O_4 percentage was calculated via the content of the Fe in NH_2-NMPs, which was obtained by analysis of the total iron concentration according to the standard colorimetric method [25] by using a spectrophotometer (722, Shanghai, China). The concentration of Cr(VI) ions in the aqueous solution was analyzed by the standard colorimetric method [26] at a wavelength of 540 nm after acidification of samples with 1 N H_2SO_4 and reaction with 1,5-diphenyl carbazide to produce a purple color complex for colorimetric measurement.

Adsorption experiments

A stock solution of chromium(VI) at concentration of 1000 mg L^{-1} was prepared by dissolving a known quantity of potassium dichromate ($K_2Cr_2O_7$) in ultrapure water. Batch adsorption studies were performed by mixing 0.05 g NH_2-NMPs with 40 mL $K_2Cr_2O_7$ solution of varying concentration from 50 to 1000 mg L^{-1} in a 100-mL stopper conical flask. 1.0 mol L^{-1} HCl and 0.5 mol L^{-1} NaOH solutions were used for pH adjustment. To investigate the effect of pH value, 40 mL of 50 mg L^{-1} Cr(VI) with pH ranging from 2.0 to 9.0 was mixed with 0.05 g NH_2-NMPs for 24 h to reach equilibrium. For the adsorption kinetic studies, 0.05 g NH_2-NMPs was added into 40 mL of 50 mg L^{-1} Cr(VI), samples were taken for Cr(VI) concentration measurements at specific time intervals. Adsorption isotherm studies were conducted by varying the initial Cr(VI) concentration from 50 to 1000 mg L^{-1} at temperature of 308.15 K and pH value at 2.0–2.5. For the thermodynamics studies, 0.05 g NH_2-NMPs was added into 40 mL of 200 mg L^{-1} Cr(VI) with temperature ranging from 298.15 to 338.15 K.

Adsorption data analysis

The equilibrium adsorption capacity for each adsorbent, q_e (mg g^{-1}), was determined by analyzing Cr(VI) concentration before and after the treatment and calculated by using the Eq. 1

$$q_e = \frac{(C_0 - C_e)V}{m} \quad (1)$$

where C_0 and C_e are the initial and equilibrium Cr(VI) concentrations in the solution (mg L^{-1}), m is the adsorbent dosage (mg), and V is the volume of the solution (mL), the same hereinafter.

The adsorption kinetic data obtained from batch experiments were analyzed by using a pseudo-second-order rate expressed as Eq. 2 [14]

$$\frac{t}{q_t} = \frac{1}{k_2 q_{e.c}^2} + \frac{t}{q_{e.c}} \quad (2)$$

where q_t is the amount of Cr(VI) adsorbed onto adsorbent any time t (mg g^{-1}) and k_2 is the second-order rate constant at the equilibrium (g mg^{-1} in^{-1}). Thus, by plotting t/q_t against t, the values of k_2 (slope^2/intercept), $q_{e.c}$ (1/slope) and $k_2 q_{e.c}^2$ (the initial adsorption rate (mg g^{-1} min^{-1}), 1/intercept) can be determined graphically from the slope and intercept of the revealed plots.

The Langmuir model was used to characterize the maximum adsorption capacity of the given adsorbents, which is expressed as Eq. 3 [19]

$$\frac{C_e}{q_e} = \frac{1}{K q_m} + \frac{C_e}{q_m} \quad (3)$$

where q_m and K are the Langmuir constants, which are related to the maximum adsorption capacity and apparent heat change, respectively.

The adsorption thermodynamic data obtained from batch experiments were analyzed by using Eq. 4 [27]

$$\ln K_D = -\frac{\Delta H^\theta}{RT} + \frac{\Delta S^\theta}{R} \quad (4)$$

where ΔH^θ and ΔS^θ are the values of standard enthalpy change, and standard entropy change, respectively. K_D is the distribution coefficient, which is defined as Eq. 5 [27]

$$K_D = \frac{\text{Amount of Cr(VI) adsorbed on } NH_2\text{-NMPs}}{\text{Amount of Cr(VI) in solution equilibrium}} \times \frac{V}{m} \quad (5)$$

Results and discussion

Characterization of adsorbents

The TEM, VSM, BET, XRD, and FTIR spectra of the NH_2-NMPs were recorded. The characterization of TEPA-NMPs was taken as a representative discussed as follows. The TEM image of TEPA-NMPs was shown in Fig. 2a. It revealed that the TEPA-NMPs particles were multidispersed with an average diameter of around 30 nm. It is known that magnetic particles of less than 30 nm will exhibit paramagnetism [28]. The paramagnetic properties of the TEPA-NMPs were verified by the magnetization curve measured by VSM, and the saturation moment of the synthesized particles obtained from the hysteresis loop was found to be 3.79 emu g^{-1}. The TEPA-NMPs were expected to respond well to magnetic fields without any permanent magnetization, therefore making the solid and liquid phases separate easily. The surface area measured by BET (S_{BET}) of TEPA-NMPs was measured to be 0.09 m^2 g^{-1}, which indicated that TEPA-NMPs were non-porous.

The XRD patterns of TEPA-NMPs were shown in Fig. 2b. Six characteristic peaks of Fe_3O_4 at 2θ of 30.1°, 35.5°, 43.1°, 53.4°, 57.0°, and 62.6° corresponding to their indices (220), (311), (400), (422), (511), and (400) were observed, which revealed that the binding and amino-functionalization did not cause any measureable change in the phase property of Fe_3O_4 cores. This could be attributed to the fact that the binding and amino-functionalization occurred only on the surface of the Fe_3O_4 cores to form a core–shell sturcture.

The IR spectra of OA-M, M-*co*-(GMA-MMA) and TEPA-NMPs were shown in Fig. 3. In the IR spectra of OA-M (Fig. 3a), the characteristic band of Fe_3O_4 occurs at ~589 cm^{-1}. Other typic bands can be assigned as follows: ν(–OH): ~3446 cm^{-1}, ν(–CH_2, –CH_3): ~2924 cm^{-1}, ~2853 cm^{-1}, ν(C=O): ~1630 cm^{-1} and ν(C=C): ~1429 cm^{-1}. These revealed that the Fe_3O_4 was coated with oleic acid. After co-polymerization, the characteristic absorptions of C=O groups at ~1730 cm^{-1}, C–O–C groups at ~1265 and ~1149 cm^{-1} appeared, as shown in Fig. 3b. After further amino-functionalization, the characteristic peaks of –NH– and –NH_2– groups at ~1576 and ~3365 cm^{-1} appeared, shown in Fig. 3c. This revealed that the epoxyl-of M-*co*-(GMA-MMA) had been functionalized successfully with the amino groups via ring-opening reaction.

Effect of initial concentration and pH value on the adsorption properties

The effect of initial concentration on the adsorption properties was intensively investigated for TEPA-NMPs by varying C_0 of Cr(VI) at 50, 500, and 1000 mg L^{-1}. The results were shown in Fig. 4a. Under corresponding pH value from 2.0 to 9.0, the adsorption efficiency of Cr(VI) decreased with the increase of the initial Cr(VI) concentration. The percentage of uptake Cr(VI) for TEPA-NMPs decreased from 99.9% to 16.5%, 73.9% to 11.5%, and 47.2% to 9.4% gradually with an increase of pH value from 2.0 to 9.0 for the concentration of Cr(VI) at 50, 500, and 1000 mg L^{-1}, respectively. The phenomenon could be attributed to the fact that for a fixed adsorbent dosage, the total available adsorption sites would be relatively settled, thus leading a decrease in adsorption percentage of adsorbate corresponding to the increased initial Cr(VI) concentration.

The effect of pH value on the adsorption properties was studied by mixing 40 mL of 50 mg L^{-1} Cr(VI) with 0.05 g different NH_2-NMPs by varying pH ranging from 2.0 to 9.0 for 24 h. The results were shown in Fig. 4b. As shown in Fig. 4b, the adsorption efficiency was highly pH dependent. The adsorption efficiency reached a maximum (over

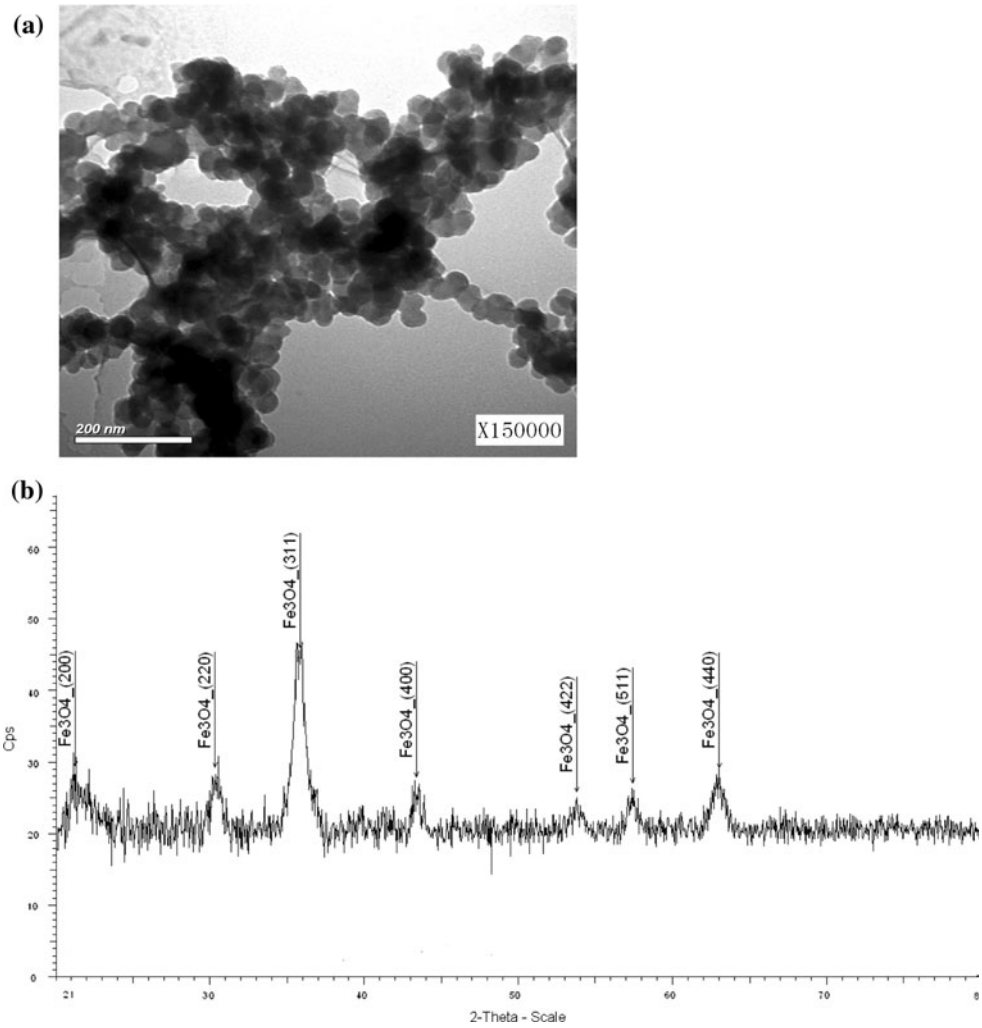

Fig. 2 TEM image (**a**) and XRD (**b**) of TEPA-NMPs nanoparticles

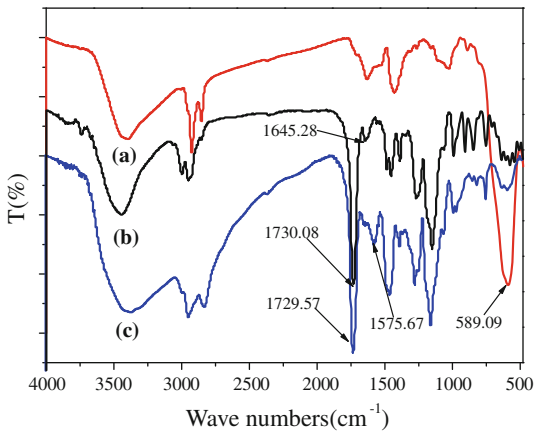

Fig. 3 FTIR adsorption spectra of (*a*) OA-M, (*b*) M-*co*-(GMA-MMA), and (*c*) TEPA-NMPs

99.9%) at pH of 2.0 for TEPA-NMPs, and pH of 2.5 for EDA-NMPs, TETA-NMPs, and DETA-NMPs, respectively. The effect of pH value on the adsorption efficiency was due to its influence on the surface properties of the adsorbent as well as different species of the Cr(VI) in aqueous solution. The species of the Cr(VI) are not only related to its concentration but also the pH value of the solution. In the case of the initial concentration of the Cr(VI) solution from 50 to 500 mg L^{-1}, Cr(VI) exists mainly in the soluble form of $HCrO_4^-$ with pH from 2.0 to 6.5 [29]. However, Cr(VI) exists mainly in the soluble forms of both $HCrO_4^-$ and $Cr_2O_7^{2-}$ at pH from 2.0 to 6.5 with the initial concentration of the Cr(VI) solution from 500 to 1000 mg L^{-1}[29]. In both cases, Cr(VI) exists mainly in soluble form of CrO_4^{2-} at pH value above 6.5. The main factor affecting this variation of adsorption efficiency in different pH value may be due to the fact that the adsorption free energy of different chromium species ($HCrO_4^-$, H_2CrO_4, and CrO_4^{2-}) varied with pH [8]. The adsorption free energy of $HCrO_4^-$ and CrO_4^{2-} is −2.5 to −0.6 kcal mol^{-1} and −2.1 to −0.3 kcal mol^{-1}, respectively [30]. The adsorption free energy of $HCrO_4^-$ is lower than that of CrO_4^{2-}, and consequently $HCrO_4^-$ is more favorably adsorbed than CrO_4^{2-} at same concentration. From the above discussion, it can be educed that Cr(VI)

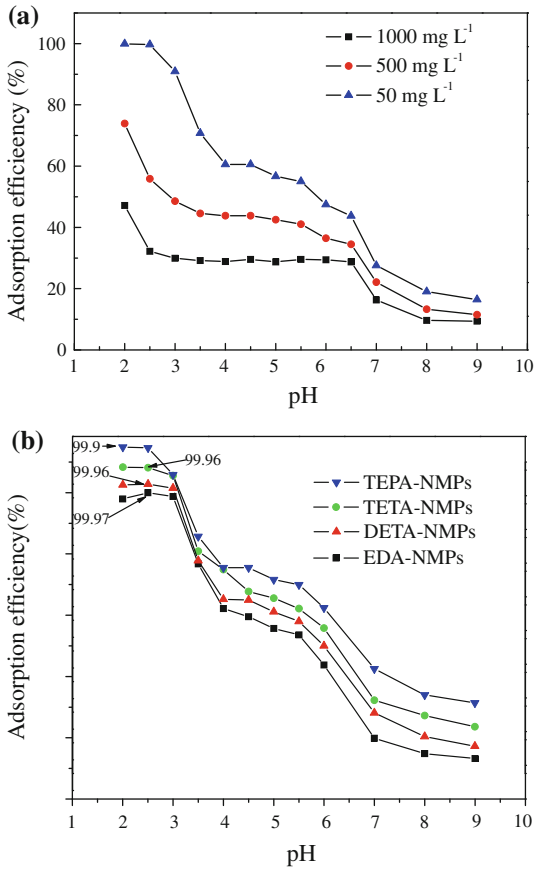

Fig. 4 **a** Effect of pH and concentration on the adsorption of Cr(VI) by TEPA-NMPs, **b** effect of pH value on the adsorption of Cr(VI) by NH_2-NMPs

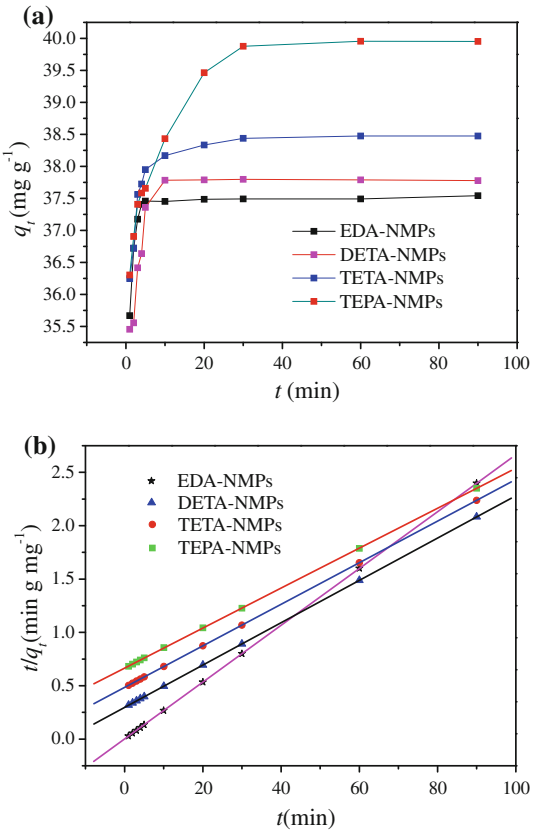

Fig. 5 **a** Kinetic studies on the adsorption of Cr(VI) by NH_2-NMPs and **b** linear plot of $t \cdot q_t^{-1}$ versus t for adsorption of Cr(VI) on NH_2-NMPs samples

was adsorbed by this adsorbent mainly in the soluble form of $HCrO_4^-$.

Adsorption kinetic studies

The effect of time on the adsorption of Cr(VI) by NH_2-NMPs was shown in Fig. 5a. It can be seen that the rate of Cr(VI) uptake was initially quite high, followed by a much slower subsequent adsorption capacity leading gradually to an equilibrium condition. Though it took 0.5 h to reach equilibrium, adsorption capacity obtained at any time (q_t) got to ~95% of the adsorption capacity at equilibrium (q_e) during the first 5 min. Since NH_2-NMPs are non-porous as characterized by BET, rapid adsorption of Cr(VI) can be realized by external surface adsorption. Because almost all of the adsorption sites exist in the exterior of the adsorbent, it is easier for the adsorbent to access these active sites, thus resulting in a rapid approach to equilibrium. At equilibrium, the adsorption capacities of Cr(VI) at initial concentration of 50 mg L^{-1} for any kind of the NH_2-NMPs were found to be at around 39.9 mg g^{-1}, therefore, the residue concentration of Cr(VI) can be reduced to less than 0.05 mg L^{-1}. This result is very promising for practical applications because there would be no need for a further treatment since the concentration of Cr(VI) in the effluent undergoing adsorption can meet the discharge requirement. Furthermore, comparing to other adsorbents such as activated carbon [31], the present NH_2-NMPs had great advantages with much shorter adsorption equilibrium time.

In order to investigate the mechanism of adsorption and potential rate-controlling steps, the adsorption kinetic data obtained from batch experiments were analyzed by using a pseudo-second-order rate equation. The linear plots of $t \cdot q_t^{-1}$ versus t for NH_2-NMPs were shown in Fig. 5b. Some important parameters, i.e., the rate constant (k_2) and the calculating equilibrium adsorption capacities ($q_{e.c}$), etc. were listed in Table 1, which indicated that the data fit the pseudo-second-order rate equations well. The values of $q_{e.c}$ obtained from the pseudo-second-order model (37.6, 37.9, 38.5, and 40 mg g^{-1}) agreed perfectly to the experimental values of q_e (37.49, 37.79, 38.47, and 39.96 mg g^{-1}) for EDA-NMPs, DETA-NMPs, TETA-NMPs, and TEPA-NMPs, respectively. Based on the assumption of pseudo-second-order model [32], the rate limiting step may be a chemical adsorption involving valence forces through sharing or exchange of electrons between adsorbent and

Table 1 The pseudo-second-order rate equations and constants of NH_2-NMPs

NH_2-NMPs	Pseudo-second-order rate equations	k_2 ((g mg^{-1}) min^{-1})	q_e (mg g^{-1})	$q_{e.c}$ (mg g^{-1})	$k_2 q_e^2$ ((mg g^{-1}) min^{-1})	R^2
EDA-NMPs	$t/q_t = 0.0266t + 0.0009$	0.7862	37.49	37.6	1111.1	1
DETA-NMPs	$t/q_t = 0.0264t + 0.0019$	0.3668	37.79	37.9	526.3	1
TETA-NMPs	$t/q_t = 0.026t + 0.0021$	0.3219	38.47	38.5	476.2	1
TEPA-NMPs	$t/q_t = 0.025t + 0.006$	0.1042	39.96	40	166.7	1

adsorbate. This further indicated that the adsorption capacities of the NH_2-NMPs adsorbents were proportional to the number of active sites on the surface [14]. It was obvious to see that the functional groups of amine increased, the number of active sites on their surface increased as well, which led to a increase in q_e for NH_2-NMPs. The initial adsorption rates decreased from 1111.1 to 166.6 mg g^{-1} min^{-1} with the functional groups of amino increased for NH_2-NMPs. These results were consistent with the findings that appeared in a chemisorption-controlled mechanism between the adsorbents surface and adsorbate ions as well [32].

Adsorption isotherms

Adsorption isotherms of NH_2-NMPs with different amino groups were obtained at the optimized temperature and pH with the initial concentration of Cr(VI) varying from 50 to 1000 mg L^{-1}. The results were shown in Fig. 6. The experimental data of all the NH_2-NMPs were well correlated with the Langmuir isotherm equation ($R^2 > 0.99$). The q_m and K values for the adsorption of Cr(VI) were listed in Table 2. It can be seen that the values of q_m increased with the increasing of nitrogen percentage in the NH_2-NMPs, i.e., the more amino groups of the NH_2-NMPs had, the higher maximum adsorption capacity would be able to be achieved, which indicated that the amino groups played a very important role in the adsorption process of Cr(VI) in aqueous solution.

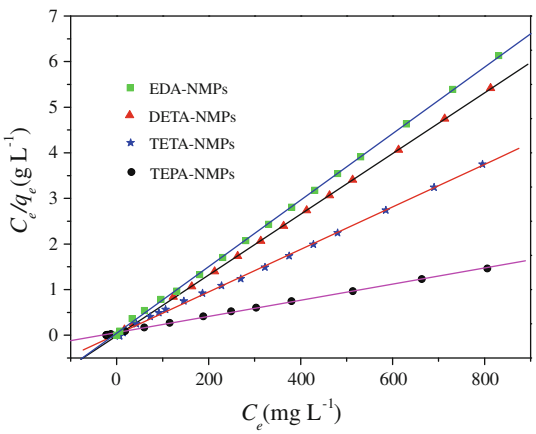

Fig. 6 Langmuir isotherms for Cr(VI) adsorption

The fundamental characteristics of Langmuir equation can be interpreted in terms of a dimensionless constant separation factor R_L, defined by Eq. 6 [33]

$$R_L = \frac{1}{1 + KC_0} \tag{6}$$

where K is Langmuir constant, and C_0 is initial concentration of Cr(VI). The value of R_L indicated the types of Langmuir isotherm of irreversible ($R_L = 0$), favorable ($0 < R_L < 1$), linear ($R_L = 1$), or unfavorable ($R_L > 1$). By calculation, R_L was between 0 and 1 for the present NH_2-NMPs with any initial concentration of Cr(VI). For instance, for the initial concentration of Cr(VI) at 50 mg/L, the R_L was 0.11, 0.04, 0.21, and 0.14 for EDA-NMPs, DETA-NMPs, TETA-NMPs, and TEPA-NMPs, respectively, which indicated that the adsorption isotherms obeyed the Langmuir rules.

Adsorption thermodynamic studies

In order to evaluate the thermodynamic parameters for adsorption of Cr(VI) on NH_2-NMPs, the adsorption studies were carried out at temperature from 298.15 K to 338.15 K, and the results were shown in Fig. 7. It can be seen that the value of distribution coefficient (K_D) for NH_2-NMPs increased with the increasing of temperature. This indicated that adsorption of Cr(VI) on NH_2-NMPs was endothermic and entropy favored in nature. The values of standard enthalpy change ΔH^θ and standard entropy change ΔS^θ, which were related to distribution coefficient (K_D), were calculated and presented in Table 3. Using the values of ΔH^θ and ΔS^θ, standard free energy changes ΔG^θ at 308.15 K for NH_2-NMPs were evaluated and the results were tabulated in Table 3 as well.

Adsorption capacity comparison

The comparison of the adsorption capacity of NH_2-NMPs with other adsorbents examined for the removal of Cr(VI) under similar conditions reported in literature were summarized in Table 4. As shown in Table 4, the present NH_2-NMPs had a much higher maximum adsorption capacity

Table 2 The Langmuir isotherms, constants and nitrogen percentage of NH_2-NMPs

NH_2-NMPs	Nitrogen percentage obtained from EA (%)	Langmuir isotherms	Langmuir constants		
			K (L mg^{-1})	R^2	q_m (mg g^{-1})
EDA-NMPs	6.09	$C_e/q_e = 0.0073C_e + 0.0443$	0.1648	0.9997	136.98
DETA-NMPs	7.94	$C_e/q_e = 0.0067C_e + 0.015$	0.4467	0.9999	149.25
TETA-NMPs	9.08	$C_e/q_e = 0.0049C_e + 0.0653$	0.0750	0.9989	204.08
TEPA-NMPs	9.89	$C_e/q_e = 0.0027C_e + 0.0219$	0.1233	0.9991	370.37

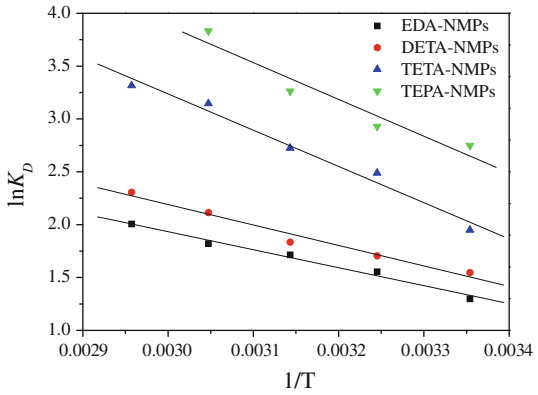

Fig. 7 Plot of ln K_D versus $1/T$ for adsorption of Cr(VI) on NH_2-NMPs samples

comparing to other adsorbents reported in literature. They should be very promising particles for the removal of Cr(VI) in wastewater.

Table 4 Adsorption capacities of various adsorbents for Cr(VI)

Adsorbents	pH	T (°C)	q_m (mg g^{-1})	Ref.
EDA-NMPs	2.5	35	136.98	This work
DETA-NMPs	2.5	35	149.25	This work
TETA-NMPs	2.5	35	204.08	This work
TEPA-NMPs	2.0	35	370.37	This work
Rice bran	2.0	30	294.1	[34]
Seed of *Ocimum basilicum*	2.0	25	205.0	[35]
Eucalyptus bark	2.0	32	45.0	[36]
Wheat bran	2.0	r.t.	35.0	[37]
Green algae Spirogyra species	2.0	18	14.7	[38]
Chlamydomonas reinhardtii	2.0	25	18.2	[39]
Maghemite nanoparticles	2.0	25	19.2	[40]
Modified jacobsite	2.0	25	31.55	[41]
Imidazole functionalized	2.5	25	152	[5]
Iron humate	~4.0	r.t.	20.0	[42]
Biomass of *Rhizopus nigrificans*	2.0	45	43.5	[43]

Adsorption mechanisms

The adsorbent properties, particularly the functional groups on the adsorbent surface, play a crucial role on the adsorption mechanisms. The most commonly reported mechanisms for adsorption of metal ions included ion exchange, electrostatic interaction, chelation, precipitation, and complexation [18, 44]. For anions, electrostatic interaction plays an important role in allowing the approach of the ions to the adsorbent surfaces. The amino groups on the adsorbent surface are easily protonated under acidic condition and are favorable for anion adsorption [45].

As aforementioned, the adsorption properties of the NH_2-NMPs were highly pH dependent, therefore, there could be electrostatic attraction and ion exchange during the process of removing Cr(VI) from wastewater by NH_2-NMPs.

The surfaces of NH_2-NMPs were covered with amino groups (–NH–, –N<, and $–NH_2$). The forms of amino groups varied at different pH. Amino groups would be protonated at pH below 10.4 as well [20]. As shown in Fig. 4b, the optimized pH value decreased from 2.5 to 2.0 for EDA-NMPs, DETA-NMPs, TETA-NMPs, and TEPA-NMPs, respectively. This phenomenon could be attributed to the fact that the more amino groups in the NH_2-NMPs there were, the more H^+ used for protonation, leading a lower optimized pH value. Under acidic conditions, amino

Table 3 Thermodynamic parameters for the adsorption of Cr(VI) onto NH_2-NMPs

NH_2-NMPs	Cr(VI) concentrations (mg L^{-1})	ΔH (kJ mol^{-1})	ΔS (J mol^{-1} K^{-1})	ΔG (kJ mol^{-1}) at 308.15 K
EDA-NMPs	200	14.15	58.52	−3.88
DETA-NMPs	200	16.09	66.5	−4.39
TETA-NMPs	200	28.53	112.5	−6.14
TEPA-NMPs	200	28.93	119.06	−7.76

groups were easier to be protonated and electrostatic attraction happened as in Eq. (7) [20]. Here, $-NH_3^+$ and $HCrO_4^-$ were taken as representatives

$$-NH_3^+ + HCrO_4^- \rightarrow -NH_3^+ \cdots\cdots HCrO_4^- \quad (7)$$

$-NH_3^+$ can also contact with Cl^-, and then ion exchange took place between $HCrO_4^-$ and Cl^- as described in Eq. 8 [7]

$$-NH_3^+Cl^- + HCrO_4^- \rightarrow -NH_3^+HCrO_4^- + Cl^- \quad (8)$$

With the increasing of the pH value, the concentration of H^+ was decreased, while the concentration of OH^- which competed with $HCrO_4^-$ was increased. So the ability of $-NH_2$ to be protonated was weakened, resulting in the decline of removal efficiency.

However, it can be seen from Fig. 4a that there was a flat for each curve with different initial Cr(VI) concentration. The higher the initial Cr(VI) concentration was, the longer the pH range of the flat appeared. This phenomenon was similar to the adsorptive behavior of poly(GMA-*co*-MMA)-EDA[21] and amino-functionalized magnetic nano-adsorbent [19] to Cr(VI) under different pH. If only electrostatic attraction and ion exchange existed, the removal efficiency should be decreased gradually with pH value increased. In order to illuminate the phenomenon, we supposed there was another interaction, i.e., coordination interaction, which compensated the lose of the removal efficiency resulting from electrostatic attraction and ion exchange with the increasing of the pH value. The presumed process of the coordination interactions for the removal of Cr(VI) by TEPA-NMPs was taken as an example and illustrated in Scheme 1.

To get a further understanding of the adsorption mechanism in this work, the FTIR (shown in Fig. 8) of $K_2Cr_2O_7$ (a), TEPA-NMPs-fresh (b), Cr-TEPA-NMPs (c), TEPA-NMPs-used (d) were recorded for comparison, where TEPA-NMPs-fresh were freshly prepared TEPA-NMPs, Cr-TEPA-NMPs were the TEPA-NMPs after adsorption to Cr(VI), as described in 2.2.2, and TEPA-NMPs-used were the TEPA-NMPs after desorption of Cr-TEPA-NMPs by 0.2 mol L^{-1} NaOH.

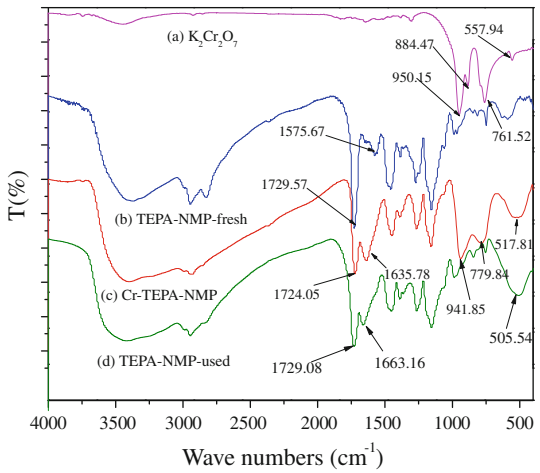

Fig. 8 FTIR adsorption spectra of (*a*) $K_2Cr_2O_7$, (*b*) TEPA-NMPs-fresh, (*c*) Cr-TEPA-NMPs, and (*d*) TEPA-NMPs-used

In the spectrum of Fig. 8a, the FTIR adsorption spectra of $K_2Cr_2O_7$, there were four characteristic bands at 950.15, 884.47, 761.52, 557.94 cm^{-1} which can be assigned to the absorptions of Cr=O and Cr–O–Cr groups.

Compared to the spectrum of $K_2Cr_2O_7$ (a), in the spectrum of Cr-TEPA-NMPs (c), the characteristic bands at 941.58 and 779.84 cm^{-1}, assigned to Cr=O and Cr–O groups, had been broadened. This may be attributed to the electrostatic attraction and ion exchange interactions between amino groups and $HCrO_4^-$ at acidic conditions. These interactions distorted the symmetric of the CrO_4^{2-} and resulted in broadening the characteristic bands of CrO_4^{2-}. Compared with the spectrum of TEPA-NMPs-fresh (b), in the spectrum of Cr-TEPA-NMPs (c), the characteristic bands of –NH– groups at 1575.67 cm^{-1} disappeared along with the appearance of the bands at 1635.78 cm^{-1}, which may be attributed to the formation of the N → Cr coordination bonds, subsequently weakened the –NH– bonding and resulted in a large shift ($\sim$60 cm^{-1}). Besides, a new band at 517.81 cm^{-1} appeared, which may be attributed to the vibration of N–Cr bond.

Moreover, compared with the two spectra of the TEPA-NMPs before adsorption (b) and after desorption (d), the

Scheme 1 The presumed process of the coordination interactions for the removal of Cr(VI) by TEPA-NMPs

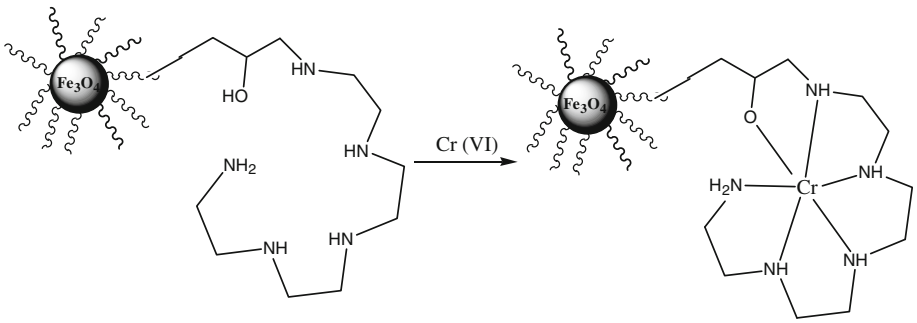

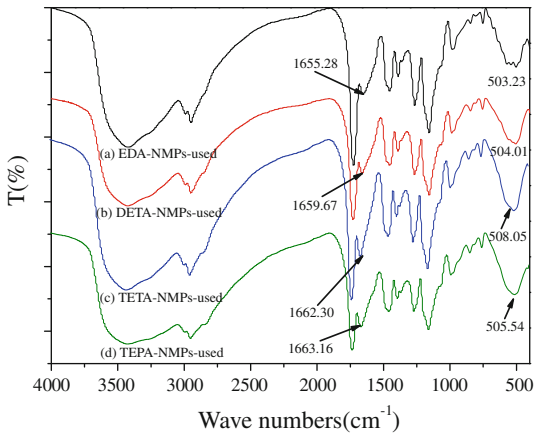

Fig. 9 FTIR adsorption spectra of (*a*) EDA-NMPs-used, (*b*) DETA-NMPs-used, (*c*) TETA-NMPs-used, and (*d*) TEPA-NMPs-used

spectrum (d) was not fully resumed to (b). In the spectrum (d), the disappearance of the bands at 950.15, 884.47, 761.52 cm^{-1}, which were assigned to Cr=O and Cr–O–Cr groups, supported the adsorption mechanism involving the electrostatic attraction and ion exchange interactions between amino groups and $HCrO_4^-$. While, the bands at 1663.16 cm^{-1}, which was attributed to the characteristic bands of the –NH– groups after the formation of the N → Cr coordination bonds, still remained. This phenomenon was also observed in the cases of the other three used NH_2-NMPs. Moreover, the bands at ~510 cm^{-1}, which can be assigned to absorption of Cr–N groups, remained as well. The FTIR spectra of the used NH_2-NMPs were summarized in Fig. 9.

From the FTIR studies discussed above, we can get a conclusion that there were coordination interactions between Cr(VI) and NH_2-NMPs during the adsorption. Overall, the adsorption mechanism of Cr(VI) by the NH_2-NMPs could be related with electrostatic attraction, ion exchange and coordination interactions.

Conclusion

In this study, a series of core–shell-structured NH_2-NMPs with different amino groups were synthesized and characterized. The effectiveness of the present NH_2-NMPs for the removal of Cr(VI) from wastewater was verified from laboratory batch tests. The removal efficiency was highly pH dependent and the optimal adsorption occurred at pH 2.0–2.5. The adsorption of Cr(VI) reached equilibrium rapidly within 30 min, and the adsorption process followed by magnetic separation leads to the rapid and inexpensive removal of Cr(VI). The data of adsorption kinetics obeyed pseudo-second-order rate mechanism well with an initial adsorption rate of 1111.1, 526.3, 476.2, and 166.7 mg g^{-1} min^{-1}, for EDA-NMPs, DETA-NMPs, TETA-NMPs, and TEPA-NMPs, respectively. The adsorption data for Cr(VI) onto NH_2-NMPs were well fitted to the Langmuir isotherm, and the adsorption process was endothermic and entropy favored in nature. Adsorption mechanism studies suggested that the adsorption of Cr(VI) onto NH_2-NMPs involved electrostatic interaction, ion exchange, and coordination interactions.

Acknowledgements We would like to thank the Ministry-of-Education Key Laboratory for the Synthesis and Application of Organic Functional Molecules (2007-KL-2007), the Zhejiang Science and Technology Bureau (2007F0045) and the Ningbo Science and Technology Bureau (2009A610002) for the financial support.

References

1. Testa JJ, Grela MA, Litter MI (2004) Environ Sci Technol 38:1589
2. Sreeram KJ, Rao JR, Sundaram R, Nair BU, Ramasami T (2004) Green Chem 2:37
3. Liu CC, Wang MK, Chiou CS, Li YS, Lin YA, Huang SS (2006) Ind Eng Chem Res 45:8891
4. Xing YQ, Chen XM, Wang DH (2007) Environ Sci Technol 41:1439
5. Park HJ, Tavlarides LL (2008) Ind Eng Chem Res 47:3401
6. Chun L, Chen HZ, Li ZH (2004) Process Biochem 39:541
7. Kulkarni PS, Kalyani V, Mahajani VV (2007) Ind Eng Chem Res 46:8176
8. Manuel PC, Jose MM, Rosa TM (1995) Water Res 29:2174
9. Hota G, Kumar BR, Ng WJ, Ramakrishna S (2008) J Mater Sci 43:212. doi:10.1007/s10853-007-2142-4
10. Gang D, Hu W, Banerji SK, Clevenger TE (2001) Ind Eng Chem Res 40:1200
11. Reichert J, Binner JGP (1996) J Mater Sci 31:1231. doi:10.1007/BF00353102
12. Sharma DC, Froster CF (1993) Water Res 27:1201
13. Oliveira EA, Montanher SF, Andrade AD, Nóbrega JA, Rollemberg MC (2005) Process Biochem 40:3485
14. Ren YM, Zhang ML, Zhao D (2008) Desalination 228:135
15. Ramanujan RV, Ang KL, Venkatraman S (2009) J Mater Sci 44:1381. doi:10.1007/s10853-006-1064-x
16. Hu J, Chen GH, Lo IMC (2006) J Environ Eng 132:709
17. Sag Y (2001) Sep Purif Method 30:1
18. Gulati R, Saxena RK, Gupta R (2002) World J Microbiol Biotechnol 18:397
19. Huang SH, Chen DH (2009) J Hazard Mater 163:174
20. Deng SB, Ting YP (2005) Environ Sci Technol 39:8490
21. Bayramoglu G, Arıca MY (2005) Sep Purif Technol 45:192
22. Deng SB, Bai RB (2004) Water Res 38:2424
23. Qus C, Yang HB, Ren DW (1999) J Colloid Interface Sci 215:190
24. Berger P, Adelman NB, Bechman KJ (1999) J Chem Educ 76:943
25. Cai BX, Chen YW (2001) Basical chemistry experiments. Science press, Beijing, China
26. Molokwane PE, Meli KC, Nkhalambayausi-Chirwa EM (2008) Water Res 42:4538
27. Ramnani SP, Sabharwal S (2006) React Funct Polym 66:902
28. Watson JHP, Cressey BA (2000) J Magn Magn Mater 214:13
29. Kang XP, Liu HH, Chen J (1999) Phys Test Chem Anal: Chem Anal 35:139
30. Weng CH, Wang JH, Huang CP (1997) Water Sci Technol 35:55
31. Sandhya B, Tonni AK (2004) Chemosphere 54:951
32. Taty-Costodes VC, Fauduet H, Porte C, Delacroix A (2003) J Hazard Mater 105:121

33. Kadirvelu K, Tharmaraiselvi K, Namasivayam C (2001) Sep Purif Technol 24:497
34. Singh KK, Rastogi R, Hasan SH (2005) J Colloid Interface Sci 290:61
35. Melo JS, D'Souza SF (2004) Bioresour Technol 92:151
36. Sarin V, Pant KK (2006) Bioresour Technol 97:15
37. Dupont L, Gallon E (2003) Environ Sci Technol 37:4235
38. Gupta VK, Shrivastava AK, Jain N (2001) Water Res 35:4079
39. Arica MY, Tuzun I, Yalcin E, Ince O, Bayramoglu G (2005) Process Biochem 40:2351
40. Hu J, Chen GH, Lo IMC (2005) Water Res 39:4528
41. Hu J, Lo IMC, Chen GH (2005) Langmuir 21:11173
42. Janoš P, Hula V, Bradnová P, Pilařová V, Šedlbauer J (2009) Chemosphere 75:732
43. Bai SR, Abraham TE (2001) Bioresour Technol 79:73
44. Ghoul M, Bacquet M, Morcellet M (2003) Water Res 37:729
45. Deng SB, Bai RB (2003) Environ Sci Technol 37:5799